CrossMark

ORIGINAL PAPER

Heterogeneous Ziegler–Natta catalysts with various sizes of MgCl2 crystallites: synthesis and characterization

Eldin Redzic[1] · Thomas Garoff[1] · Cezarina Cela Mardare[2] · Manuela List[1] ·
Guenter Hesser[3] · Leonhard Mayrhofer[1] · Achim Walter Hassel[2] · Christian Paulik[1]

Abstract A $MgCl_2$-based Ziegler–Natta catalyst was characterized using X-ray diffraction (XRD) patterns, scanning electron microscopy (SEM) and transmission electron microscopy (TEM) and IR spectra. We focused on the XRD reflection at $2\theta = 50°$ to determine the thickness of $MgCl_2$ crystals, and validated these results with TEM pictures. SEM pictures were taken in order to measure the size of the nanoparticles formed by the $MgCl_2$ crystals. Several compounds were synthesized for comparison and to aid interpretation of the infrared (IR) spectra. The catalysts were prepared by precipitating $MgCl_2$, which was used as support material and subsequently treated with $TiCl_4$. The thickness of the catalyst crystals was calculated from the XRD reflection at $2\theta = 50°$. Changing the precipitation temperature within a range from 40 to 90 °C altered the thickness of the $MgCl_2$ crystal plates. The maximum thickness of 7 nm was achieved at a precipitation temperature of 60 °C. The SEM pictures showed that the nanoparticles had a diameter of ~200 nm. A crystal base unit had a volume that corresponded to that of a sphere of 3.5 nm radius. Thus, we estimated that a typical catalyst particle with a diameter of 20 µm contained about one million nanoparticles, each of which consisted of about 25,000 $MgCl_2$ crystal units.

✉ Eldin Redzic
eredzic.chem@gmail.com

[1] Institute for Chemical Technology of Organic Materials, Johannes Kepler University Linz, 4040 Linz, Austria

[2] Christian Doppler Laboratory for Combinatorial Oxide Chemistry at the Institute for Chemical Technology of Inorganic Materials, Johannes Kepler University Linz, 4040 Linz, Austria

[3] Center for Surface and Nanoanalytics, Johannes Kepler University Linz, 4040 Linz, Austria

Introduction

In chemical industry, Ziegler–Natta catalysts are used to produce large volumes of polyethylene and polypropylene [1–3]. These catalysts produce a polymer material with a rather broad molecular weight distribution indicating that the catalysts have a structure of at least five different types of active sites [4–6]. The main components of these catalysts are: $MgCl_2$ as support material, $TiCl_4$ as the active transition metal, and triethylaluminum ($AlEt_3$, TEA) as co-catalyst. The $MgCl_2$ support material must be in a disordered, amorphous crystal state to enable the $TiCl_4$ to link via coordination bonds to the edges of the $MgCl_2$ crystal plates and thereby create active polymerization centers. The amorphous structure of the $MgCl_2$ support material is created by chemical activation in the course of catalyst synthesis. $AlEt_3$ acts as a co-catalyst and activates the titanium (Bahri-Laleh model) [7] by shifting an ethyl group to the titanium (Stukalov reaction) [8, 9]. Polymerization starts from the ethyl group that is bound to the titanium (Cossee and Trigger mechanisms) [10–12]. Coordination of the titanium to the amorphous $MgCl_2$ results in high polymerization activity of the titanium.

Numerous studies have sought to determine the optimal structure of the $MgCl_2$ support material of Ziegler–Natta catalysts and to describe the different types of active sites [13]. X-Ray diffraction (XRD) using a wavelength of 1.5406 Å has been employed to describe the activation of the catalyst components. Inactivated $MgCl_2$ material has an XRD pattern with a strong dominant reflection at 15° 2θ, which gives the height of the crystal and indicates that

IPPI Springer

inactivated $MgCl_2$ has a needle-like structure [14]. At 30° 2θ and 35° 2θ, inactivated $MgCl_2$ exhibits intense intermediate reflection peaks which result from the diagonal planes in the needle-like structure. The final significant reflection peak is at 50° 2θ; compared to the other peaks of inactivated $MgCl_2$, it is usually much smaller and indicates the thickness of the $MgCl_2$ crystal [15].

On activation of the $MgCl_2$ support material, the most drastic changes in the crystal structure can be seen on the left half of the XRD pattern. The reflection peak at 15° 2θ is strongly reduced, which suggests that the needle-like structure of the $MgCl_2$ crystals collapses almost completely, leaving only 5–10 crystal plates stacked on top of each other in the activated material. The intensities of the intermediate reflection peaks also decrease at 30° 2θ and 35° 2θ, and additionally the peaks merge and form an intermediate halo that indicates strong disorderliness in the $MgCl_2$ material [15].

The only reflection peak that remains almost unchanged by the activation process of the $MgCl_2$ material is 50° 2θ; suggesting that the thickness of $MgCl_2$ crystal plates is almost the same as in inactivated $MgCl_2$.

Since most of the changes in $MgCl_2$ crystals during the activation process are thought to be related to the destruction of their needle-like structure, most X-ray studies in this area have focused on the degradation of the reflection at 15° 2θ and on the degradation and halo formation between 30° 2θ and 35° 2θ reflection peaks in order to explain the increasing disorder in the structure of the $MgCl_2$ support material. Little or no attention has been paid to the reflection at 50° 2θ, probably since it usually remains largely unaffected by the activation process.

In this study, a typical $MgCl_2$-based Ziegler–Natta polyethylene catalyst was characterized by interpreting the XRD patterns, SEM and TEM pictures and IR spectra of the catalyst and the $MgCl_2$ support material. We focused on the XRD at 50° 2θ to determine whether additional information can be gained from the crystallographic data.

A typical Ziegler–Natta polyethylene catalyst was prepared for this investigation by first precipitating, and concurrently chemically activating the $MgCl_2$ support material via a reaction between magnesium alcoholate [$Mg(OR)_2$] and ethylaluminum dichloride ($EtAlCl_2$, EADC). The final catalyst was obtained by treating this support material with titanium tetrachloride ($TiCl_4$). In this treatment step, the titanium is linked to the support material via coordination bonds. We varied the synthetic conditions in terms of temperature and rate of addition of alcohol to determine whether this causes a significant change in the thickness of $MgCl_2$ support material and thus of the final catalyst.

Further, TEM pictures were acquired to verify the results of the XRD measurements. SEM pictures were used to find out whether a correlation exists between the size of the nanoparticles [16] in the produced material and the crystal thickness measured by X-ray at 50° 2θ. With the help of IR spectroscopy the positions of the chlorine and the alchoholate groups on Mg, Al and Ti were determined. Compounds were prepared to interpret and compare the IR spectra of the support material and the catalysts. Our aim was to discover whether there was a clear change in the chemical composition of the support material due to the titanation process carried out in the last catalyst synthesis step. Finally, we used a fast polymerization method to demonstrate that the catalyst contained active titanium.

Experimental

Model compounds

Strictly inert conditions were used in all synthesis steps when preparing the model compounds, the support materials, and the catalysts. Nitrogen (5.0, Linde, Germany) was used to create an inert atmosphere and inert conditions for characterization of these materials. In handling of the KBr tablets for IR measurements, it was not possible to achieve totally inert conditions, as the tablets had to be transferred into the IR instrument after their preparations. Consequently, an absorption band between 3200 and 3500 cm^{-1} due to absorbed moisture could be seen in all IR spectra of the KBr tablets. This moisture absorption also shifted all metal–oxygen absorption peaks in the IR spectra to lower wavelengths. All reagents were of analytical grade.

Butyloctylmagnesium (Chemtura, USA), ethylaluminum dichloride (AcroSeal, USA), diethylaluminum chloride (Sigma Aldrich, USA), triethylaluminum (Aldrich, USA) and titanium tetrachloride (Aldrich, USA) were used as provided by the manufacturer. All monomers and solvents were purified in custom-made purification columns before polymerization process. Ethene (purity >99.9 %, obtained from Air Liquide) was purified by passing through three purification columns, first through a bed of oxidized BASF R3-16 catalyst (CO scavenging to CO_2), second through reduced BASF R3-16 catalyst (absorption of O_2), third through molecular sieves (3A, 4A, 13X, obtained from Sigma-Aldrich) to physically absorb CO_2, H_2O, and other impurities and finally passed through a 50/50-combination of Selexorb-types COS and CD (Alcoa) for removing COS, H_2S, PH_3 and oxygenates, e.g., ethers, alcohol, aldehydes, carbonyls, ketones, and peroxides. Hydrogen, nitrogen (purity >99.999 %, Linde), and heptane (purity >95 %, VWR) were purified over reduced BASF R3-11 catalyst and molecular sieves (13X, 4A, 3A). To achieve an optimum purification, all columns containing BASF catalysts were heated to 200 °C, except the columns for heptane, which were heated to 60 °C because of its vapor pressure.

The purity of the compounds cleaned by this procedure was sufficiently high, so no additional treatment by Na or CaH_2 was needed.

One of our aims was to use the IR spectra of the support material and the catalysts to localize the alcoholate, chlorine and ethyl groups in the product, more precisely and to determine in what quantities they were bound to Ti, Mg or Al. To be able to interpret the IR spectra of the support
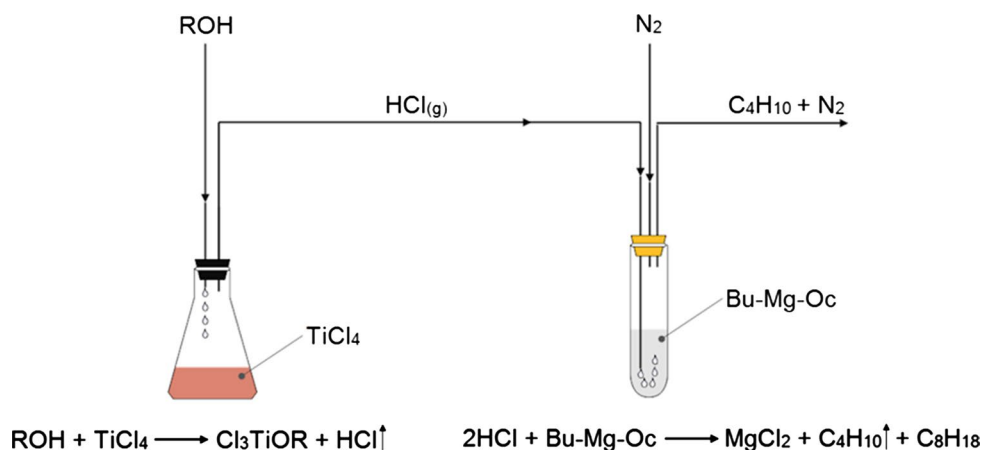
material and the catalysts, we prepared model compounds (Table 1). IR spectra of these model compounds were recorded, and their characteristic absorption peaks were identified.

Magnesium dichloride was prepared using a 150 mL glass reactor (Fig. 1). The reactor was constructed such that it could be placed in a centrifuge, where precipitate and liquid phase could be separated efficiently. An amount of

Table 1 List of model compounds prepared to interpret IR spectra

Model compounds	Formula	Reaction
Diethyl-aluminum-(2-ethyl-hexanolate)	Et_2AlOR	Reaction between triethylaluminum and 2-ethyl-hexanol at molar ratio 1:3
Ethyl-aluminum-di-(2-ethyl-hexanolate)	$EtAl(OR)_2$	Reaction between triethylaluminum and 2-ethyl-hexanol at molar ratio 1:2
Aluminum-tri-(2-ethyl-hexanolate)	$Al(OR)_3$	Reaction between triethylaluminum and 2-ethyl-hexanol at molar ratio 1:1
Aluminum-chloride-di-(2-ethyl-hexanolate)	$ClAl(OR)_2$	Reaction between diethylaluminum chloride and 2-ethyl-hexanol at molar ratio 1:2
Aluminum-dichloride-(2-ethyl-hexanolate)	Cl_2AlOR	Reaction between ethylaluminum dichloride and 2-ethyl-hexanol at molar ratio 1:1
Ethyl-aluminum-dichloride	$EtAlCl_2$	A commercial 1.0 M toluene solution of ethylaluminum dichloride was used
Ethyl-aluminum-(2-ethyl-hexanolate)-chloride	$EtAl(OR)Cl$	Reaction between diethylaluminum chloride and 2-ethyl-hexanol at molar ratio 1:1
Di-ethyl-aluminum-chloride	Et_2AlCl	A commercial 1 M *n*-heptane solution of diethylaluminum chloride was used
Titanium-tetra-(2-ethyl-hexanolate)	$Ti(OR)_4$	Reaction between titanium tetrachloride and 2-ethyl-hexanol at molar ratio 1:4
Titanium-tri-(2-ethyl-haxanolate)-chloride	$ClTi(OR)_3$	Reaction between titanium tetrachloride and 2-ethyl-hexanol at molar ratio 1:3
Magnesium-di-(2-ethyl-hexanolate)	$Mg(OR)_2$	Reaction between butyloctylmagnesium and 2-ethyl-hexanol at molar ratio 1:2
Magnesium dichloride	$MgCl_2$	Reaction between hydrochloric acid and butyl-octyl-magnesium at molar ratio 2:1
$MgCl_2$-EtAl(2-ethyl-hexanolate)$_2$	$MgCl_2$-$EtAl(OR)_2$	Reaction between magnesium-dichloride and 2-ethyl-hexanol at molar ratio 1:1; the products were then reacted with tri-ethyl-aluminum at molar ratio 2:1
$MgCl_2$-Ti-Cl$_3$-(2-ethyl-hexanolate)	$MgCl_2$-$TiCl_3$ (OR)	Reaction between magnesium-dichloride and 2-ethyl-hexanol at molar ration 2:1; the products were then reacted with titanium-tri-chloride-(2-ethyl-hexanolate) at molar ratio Mg/Ti 2:1

Fig. 1 The experimental setup used for preparation of $MgCl_2$

$$ROH + TiCl_4 \longrightarrow Cl_3TiOR + HCl\uparrow$$

$$2HCl + Bu\text{-}Mg\text{-}Oc \longrightarrow MgCl_2 + C_4H_{10}\uparrow + C_8H_{18}$$

4.3057 g (5.2465 mmol Mg) of a 20 % *n*-heptane solution of butyloctylmagnesium (BOMAG) was introduced into the glass reactor. The reactor was equipped with an outlet via an oil lock. An amount of 4.9816 g (26.2325 mmol) of $TiCl_4$ was introduced into another glass reactor that was connected to the first reactor via a pipeline. The $TiCl_4$ was diluted by adding 10 mL of *n*-heptane. Over a period of 30 min, 8.22 mL of 2-ethyl-hexanol was added dropwise at 90 °C into the reactor containing $TiCl_4$. To improve the release of HCl, the temperature was increased to 90 °C. Reaction of the alcohol with $TiCl_4$ yielded HCl gas, which passed through the pipeline and entered into the reactor containing the magnesium-alkyl, resulting in its chlorination and finally in precipitation of $MgCl_2$ (0605-1). After the addition was completed, the $MgCl_2$ precipitate was separated from the liquid by centrifugation. The $MgCl_2$ was washed once at room temperature with 10 mL *n*-heptane and next with 10 mL pentane, and it was subsequently dried under a stream of nitrogen at 50–60 °C. A tablet consisting of 200 mg KBr and 2 mg of the $MgCl_2$ precipitate was obtained and used for measuring the IR absorption spectrum.

Our procedure for synthesizing the Ziegler–Natta PE catalyst followed a typical industrial procedure that can be found in patented literature [17], and it also resembles procedures described in other publications [18, 19] and to some extent the recipe provided by Wang et al. [20]. The carrier synthesis described by Nakayama et al. [21] is an example of a support material preparation that resembles the recipe used in this study. The carrier material produced for the immobilization of homogeneous catalysts, described by Severn et al. also has a composition corresponding to the support material produced in our study [22].

Preparation of magnesium alcoholate

A magnesium alcoholate solution was prepared according the following procedure: under inert conditions, 10.0 g (18.1 mmol) of a 20.0 % toluene solution of butylethyl magnesium (BEM) was introduced into a glass reactor. Alternatively, 14.9 g (18.1 mmol) of a 20.3 % *n*-heptane solution of BOMAG was introduced. A volume of 10 mL *n*-heptane was added to reduce viscosity. Over a period of 20 min, a mass of 4.34 g (33.2 mmol) of 2-ethyl-hexanol (ROH) was added dropwise into the reactor while mixing. The temperature was kept between 20 and 25 °C at all times. The ROH/Mg molar ratio was 1.83. After complete addition, the reaction solution was allowed to stabilize for an hour at room temperature. The main part of the reaction was:

$$Bu_{1.5} - Mg - Oc_{0.5} + 2\,ROH \rightarrow Mg(OR)_2 \\ + 1.5\,BuH_{(g)} + 0.5\,OcH_{(l)} \tag{1}$$
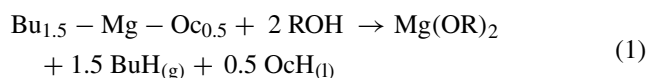
Precipitation of $MgCl_2$ carrier material

The reactor system described above was used to prepare both the $MgCl_2$ support material and the catalyst. 9.34 g (18.1 mmol) of a 1.80 M toluene solution of EADC was introduced into this reactor under inert conditions. Alternatively, 14.9 g (18.1 mmol) of a 0.90 M *n*-heptane solution of EADC was introduced. The aim of our study was to adjust $MgCl_2$ crystal thickness by varying the precipitation temperature or the EADC/$Mg(OR)_2$ ratio, because small catalyst particle size, and thus often low crystal thickness can be achieved by precipitation. It is assumed that small $MgCl_2$ crystals have more defects where Ti can form active centers, which in turn leads to higher activity. The precipitation conditions were varied by which the $MgCl_2$ support material was created in order to adjust catalyst crystal size and thereby catalyst performance. In the first test series, the temperature in this precipitation step was selected between 40 and 100 °C, and in the second test series the EADC/$Mg(OR)_2$ ratio was varied within the range 0.5–2. The magnesium alcoholate solution was then added dropwise into the reaction solution while mixing. A white precipitate started to form after about 25 % of the magnesium alcoholate solution had been added into the reactor. The total addition time was 20 min. The precipitation reaction was according to the following scheme:
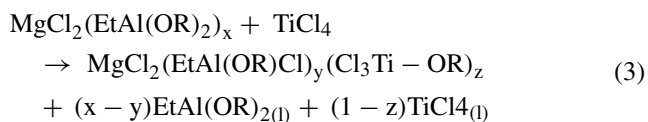
$$Mg(OR)_2 + EtAlCl_2 \rightarrow MgCl_2(EtAl(OR)_2)_{x(s)} \\ + (1-x)EtAl(OR)_2 \tag{2}$$
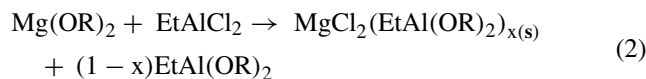
The precipitated amount of $MgCl_2$ was dependent on the reaction conditions. According to Chien et al. [23]. the "x" in the precipitate of $MgCl_2(EtAl(OR)_2)_x$ can be any value between 0 and 1, as it is not a stoichiometric compound like $TiCl_3(AlCl_3)_{0.33}$ or $MgCl_2(H_2O)_6$. The composition of the neutral complex between $MgCl_2$ and $EtAl(OR)_2$ would produce a soluble product $MgCl_2(EtAl(OR)_2)_3$.

After complete addition of the $Mg(OR)_2$, the reactants were allowed to react with each other for 30 min at 60 °C. When precipitation of the $MgCl_2$ carrier had finished, the precipitate was separated from the liquid phase in a centrifuge for 5 min at 2000 rpm. Subsequently, the precipitate was washed twice with 20 mL portions of *n*-heptane at 60 °C for 20 min. Support material intended for composition investigation was washed at room temperature with 20 mL of hexane and then dried under a stream of nitrogen at 40–60 °C.
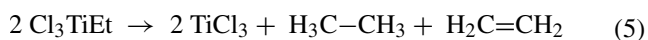
Synthesis of the Ziegler–Natta catalyst

Catalyst preparation started by producing the support material in a slurry form in 7 mL of *n*-heptane. Next, 1.72 g (9.07 mmol) $TiCl_4$ diluted with 10 mL of *n*-heptane were

added. The vial that had contained the $TiCl_4$ was washed with 3 mL of *n*-heptane, which was then added into the reactor to ensure complete transfer of the $TiCl_4$. The reaction components were then allowed to react for 30 min at 60 °C. In this reaction, the $EtAl(OR)_2$ was partially washed out from the precipitate and exchanged with $TiCl_4$. In addition, some of the alcoholate groups shifted to the titanium according to:

$$MgCl_2(EtAl(OR)_2)_x + TiCl_4$$
$$\rightarrow MgCl_2(EtAl(OR)Cl)_y(Cl_3Ti-OR)_z \quad (3)$$
$$+ (x-y)EtAl(OR)_{2(l)} + (1-z)TiCl4_{(l)}$$

According to Chien et al. [23] the presence of $EtAl(OR)_2$ in the precipitate also causes part of the titanium to reduce from Ti(IV) to Ti(III) via the reactions:

$$TiCl_4 + EtAl(OR)_2 \rightarrow Cl_3TiEt + ClAl(OR)_2 \quad (4)$$

$$2\,Cl_3TiEt \rightarrow 2\,TiCl_3 + H_3C-CH_3 + H_2C=CH_2 \quad (5)$$

After completion of the reaction, the catalyst was separated from the solution by centrifugation for 5 min at 2000 rpm. Subsequently, the catalyst was washed once with 20 mL of *n*-heptane for 20 min at 60 °C and then with 20 mL of hexane at room temperature. Finally, the catalyst was dried under a stream of nitrogen at 40–50 °C. The yield was about 2 g of catalyst per synthesized batch. XRD of the catalyst was then measured, and IR spectra, SEM and—in some cases—also TEM pictures of the catalyst and the carrier were recorded. The catalysts were also tested for active titanium in a polymerization quick test [24]. The synthetic content and catalyst codes are given in Table 2.

As previously mentioned, we sought to investigate the effects of small changes in crystal structures in relation to the synthetic conditions of the catalyst. First, the temperature was varied between 40 and 90 °C, and then the addition rate of the $Mg(OR)_2$ solution into the reactor was varied between 1 min and 300 min. A few tests were performed using a temperature of 120 °C in the titanation step.

Further, we increased the amount of $EtAlCl_2$ in the precipitation step, and finally treated the catalyst with $TiCl_4$ a second time at $TiCl_4/MgCl_2$ molar ratio of 12.

IR spectra

IR Analyses were performed on a Thermo Fisher Scientific Nicolet iN10MX (Thermo Scientific, USA) microscope with an iN10Z unit using attenuated total reflection (ATR) mode or transmission mode with CaF_2 windows or KBr tablets. Spectra were recorded in the range of 400–4000 cm^{-1} at a resolution of 4 cm^{-1}. KBr tablets were prepared from a blend of 200 mg KBr and 2 mg sample. When CaF_2 windows were used, a drop of the sample solution (in *n*-heptane) was placed between the two windows.

X-ray diffraction (XRD) patterns

XRD measurements were performed using a Philips Pro X'Pert (PANalytical, Netherlands) system with CuKα radiation and a wavelength $\lambda = 154.056$ pm. The X-ray tube was powered using an acceleration voltage of 45 kV and a current of 40 mA. The catalyst powders were placed in a specially designed holder that allowed covering the powder with a Mylar film, which was necessary to reduce the exposure to moisture during the measurement and thus to hinder the formation of hydrated or hydroxide phases. All diffractograms were acquired in Bragg–Brentano geometry, with a step size of 0.0021° and 40 s per step. The crystallite grain size was determined based on the peak broadening using the single-line method and the Scherrer formula:

$$\Gamma = \frac{\kappa\lambda}{D\cos\theta} \quad (6)$$

where Γ is the full width at half maximum (FWHM) of a diffraction line, K denotes the Scherrer constant, which was considered to be 0.9 (assuming spherical particles), 2θ is the diffraction angle, and D is the grain diameter D [25]. In general, when determining the grain size based on peak

Table 2 Synthesis setup and catalyst codes

Catalyst code	$Mg(OR)_2$ addition temperature (°C)	$Mg(OR)_2$ addition (time/min)	$EtAlCl_2$/Mg molar ratio	Titanation temperature (°C)	Second $TiCl_4$ treatment $TiCl_4/MgCl_2$ at 60 °C
0206-1s	60	20	1:1	Non	Non
0206-2	60	20	1:1	60	Non
0406-1	80	20	1:1	120	Non
0606-1	70	20	1:1	70	Non
1006-1	90	20	1:1	90	Non
1006-2	40	20	1:1	40	Non
1106-1	60	20	2:1	60	Non
1706-1	60	20	1:1	60	12

broadening, also the broadening related to the XRD equipment and that caused by the microstrain must be taken into consideration [26]. Equation (6) is a good approximation in the case of extensive broadening (small crystallite size) when no large microstrain is present. The broadening related to the equipment was determined using a highly crystalline silicon powder and evaluated based on the peak at $2\theta = 28.46°$. The peak broadening value obtained for silicon (0.0854°) was deducted from the peak broadening values obtained for the catalysts powders.

SEM pictures

SEM pictures allow the size of the nanoparticles in a Ziegler–Natta catalyst to be estimated [14, 16, 27]. For example, Busico et al. [28]. estimated that the size of the nanoparticles of their PP catalyst, which was ball-milled for 20 h, was about 100 nm. Additionally, SEM images can be used to estimate the pore structure of catalyst. For instance, Nejad et al. [26] stated on the basis of their SEM investigations that a catalyst with a large pore structure of 50–100 nm produces good replica in PE polymerization, whereas for pore structures between 20 and 50 nm fine porosity, and for catalyst pore structures as small as 10–20 nm, polymerization yields only fine particles.

The SEM images were acquired using a ZEISS 1540XB CrossBeam instrument (Carl Zeiss Microscopy, Germany) with a field emission filament, using an acceleration voltage of 2 kV with a SE2-Detector. The catalyst samples were applied to the sample holder and covered with a Mylar® film in a glove box to prevent hydration from the atmosphere prior to the SEM investigations.

TEM pictures

The catalyst samples were suspended in *n*-heptane and then further diluted with *n*-heptane to cause disintegration of the catalyst particles into nanoparticles and basic $MgCl_2$ crystalline units. A drop of this diluted suspension was placed on a membrane covering a copper grid. The sample was then put in a desiccator to dry. All sample preparation steps were carried out under strictly inert conditions. TEM images were acquired on a Jeol-2011 TEM with a LaB6-filament with an acceleration voltage of 200 kV (Jeol, Japan) [29].

Polymerization quick test

The quick test was performed in a micro-reactor equipped with a video-microscope [24, 30]. The quick test was started by pre-contacting catalyst and co-catalyst (TEA) for 30 min at an Al/Ti molar ratio of 25. 10 μL of concentrated TEA was placed next to the polymerization area

for scavenging. The activated catalyst was placed on the polymerization table by means of a micropipette, and catalyst particles without contact to each other were chosen for evaluation. After flushing the feed pipe five times with vacuum and ethylene, ethylene was injected to start the polymerization. A constant ethylene pressure of 20 bar (2 MPa) was applied, and the polymerization temperature was kept at 70 °C.

Results and discussion

IR results

IR absorption bands in the model compounds

For model compounds with more than one ethyl ligand group, inert conditions were created by enclosing the sample between CaF_2 windows during measurement. The progress of the reaction between 2-ethyl-hexanol and the ethyl-aluminum group could be tracked by observing the disappearance of the broad absorption band between 3200 and 3500 cm^{-1} (with a maximum at 3420 cm^{-1}) [23, 31, 32] originating from the –OH group in the added 2-ethyl-hexanol. The situation was the same for tracking the alcohol reaction with $TiCl_4$ and with butyl-ethyl-magnesium. The results indicated quantitative reactions in all cases in which TEA, EADC and BEM were involved. No remaining absorption of an –OH group between 3200 and 3500 cm^{-1} was observed for these reaction products. In contrast, all reaction products originating from DEAC and the alcohol showed a flat and broad absorption starting from 3000 cm^{-1} and continuing up to 3500 cm^{-1}. However, since the same flat absorption band was also observed for the DEAC reagent itself, the –OH absorption seen in the reaction product most probably originated from the Et_2AlCl reagent and did not indicate an incomplete reaction. The only case in which an incomplete alcohol reaction was observed was that involving $TiCl_4$. In both instances in which $TiCl_4$ was used, a remaining absorption between 3200 and 3500 cm^{-1} could be seen, which indicated that unreacted alcohol was present in the reaction mixture. Generally only two of the chlorine atoms of $TiCl_4$ tended to react, even in the presence of excess alcohol. Hence, the results indicated that an Al–Et group reacted more readily with alcohol than a Ti–Cl group in $TiCl_4$.

The positions of the Al–OR, Al–Et, Al–Cl and Ti–OR groups were determined using the IR spectra and ignoring all the absorption peaks originating from 2-ethyl-hexanol and the solvent. The Al–OR group showed strong absorption at 635 and 1037 cm^{-1}, and weaker absorption at 906 and 1120 cm^{-1} (Fig. 2). However, the strong absorption at 635 cm^{-1} was relatively close to the limits of accurate measurement of the
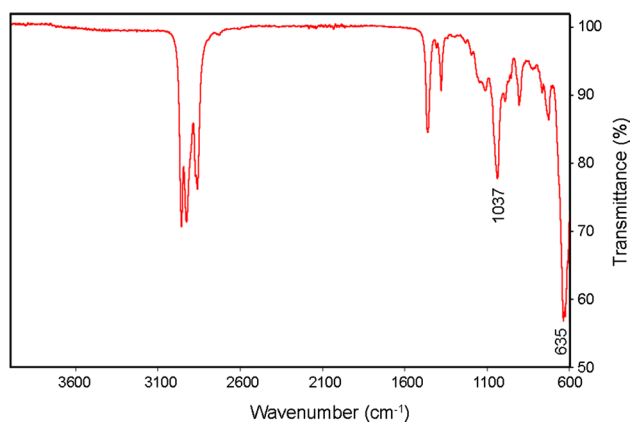
Fig. 2 IR spectrum of EtAl(OR)$_2$ showing strong absorption at 635 and 1037 cm^{-1}. The 635 cm^{-1} absorption peak is relatively close to the measurement limit of the instrument, so its position should be regarded only as indicative. Additionally, the normal hydrocarbon peaks can be seen, but no sign of moisture has been detected

Table 3 Absorption peaks identified for the Al–Et, Al–OR, Al–Cl and the Ti–OR groups in the model compounds

Model compound	Absorption at (cm^{-1})	Absorbing group	Comment
Al(Et)$_3$	987	Al–CH$_2$–	
	1055	Al–CH$_2$–	
	1100	Al–CH$_2$–	
(Et)$_2$AlOR	991	Al–CH$_2$–	
	1055	Al–CH$_2$–	
	1100	Al–CH$_2$–	
EtAl(OR)$_2$	635	Al–O–CH$_2$–	Strong
	906	Al–O–CH$_2$–	
	1120	Al–O–CH$_2$–	
Al(OR)$_3$	635	Al–O–CH$_2$–	
	906	Al–O–CH$_2$–	
	1120	Al–O–CH$_2$–	
ClAl(OR)$_2$	635	Al–O–CH$_2$–	
	1116	Al–O–CH$_2$–	
	872	Al–Cl	
Cl$_2$AlOR	872	Al–Cl	
Cl$_2$AlEt	990	Al–CH$_2$–	Al–Cl not seen
EtAl(OR)Cl	634	Al–O–CH$_2$–	Strong
ClAlEt$_2$	986	Al–CH$_2$–	
Ti(OR)$_4$	698	Ti–O–CH$_2$–	
	845	Ti–O–CH$_2$–	
	1002	Ti–O–CH$_2$–	
ClTi(OR)$_3$	718	Ti–O–CH$_2$–	Strong
	845	Ti–O–CH$_2$–	Strong
	1006	Ti–O–CH$_2$–	
Mg(OR)$_2$	595	Mg–O–CH$_2$–	Inconclusive
MgCl$_2$	1633	Mg–Cl/moisture	Strong
MgCl$_2$–EtAl(OR)$_2$	1635	Mg–Cl/moisture	Strong
	1051	Mg–O(Al)–CH$_2$–	
	630	Al–O–CH$_2$	
MgCl$_2$–Ti Cl$_3$(OR)	1635	Mg–Cl/moisture	Strong
	1073	Mg–O(Ti)–CH$_2$–	Possible
	603	Mg–O–CH$_2$–	Inconclusive

instrument, so the position of this absorption peak must be regarded as the only confirmation. The Al–Et group showed moderately weak absorptions at 987, 1055 and 1100 cm^{-1} and the Al–Cl group showed absorption only at 872 cm^{-1}.

The Ti–OR group showed strong absorption at 845 and 718 cm^{-1} and weaker absorption at 1006 cm^{-1}. The stretching vibration of a single 2-ethyl-hexanolate group on titanium chloride showed up at 1050 cm^{-1} according to Gupta et al. [33] and between 1110 and 1130 cm^{-1} according to Kissin et al. [11], so in several cases there seemed to be disagreement not only between our results and published results, but also between the values published in different articles. According to Thongdonjui et al. Ti–Cl exhibits absorption at 466 and 618 cm^{-1} [19]. For the model compounds presented in this work, these absorptions peaks were outside the measuring range of the instrument used.

The results obtained for the model compounds indicated that the IR spectrum was a valid basis for determining whether the alcoholate group was attached to Al or to Ti because it exhibited strong absorption peaks in totally different locations in these cases. However, it turned out that forming a complex with MgCl$_2$ caused a change in the absorption of the model compound. Table 3 lists the absorption peaks identified for the model compounds.

Interference of moisture with the IR results of Mg complexes

The reaction between the magnesium-alkyl and 2-ethyl-hexanol was strongly exothermic, thus causing a temperature rise. Towards the end of the alcohol addition, the reaction mixture turned into a gel with higher viscosity. The IR spectrum of this complex is shown in Fig. 3. The spectrum

of the Mg(OR)$_2$ complex shows a strong absorption peak at 1095 cm^{-1}. This absorption peak originates most probably from the Mg–O–CH$_2$– bond. An absorption peak at the right end of the spectrum at 589 cm^{-1} is very close to the measuring limits of the instruments and must therefore be regarded as only confirmation with respect to its position. According to Ault [34], the main absorption of Mg–C bonds should appear between 530 and 550 cm^{-1}, which indicates that the absorption peaks at the right side of our Mg(OR)$_2$ spectrum originates from the unreacted part of the added MgR$_2$. The absorption band of the free –OH group in the added alcohol between 3200 and 3500 cm^{-1} disappeared completely, suggesting a quantitative reaction between the Mg-alkyl and the alcohol. According to Thongdonjui et al. and Zohuri et al. the Mg–O–Et group shows strong absorption at 1449 cm^{-1} and weaker absorption at 1632 cm^{-1} [19, 35]. This could not be confirmed in our investigation. The *n*-heptane solvent
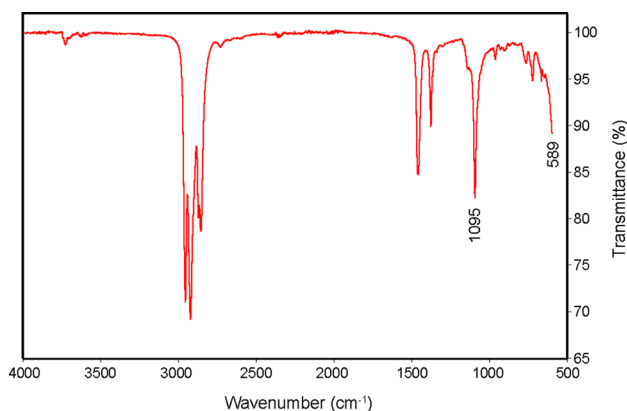
Fig. 3 IR spectrum of Mg(OR)$_2$ directly after preparation, showing no sign of moisture

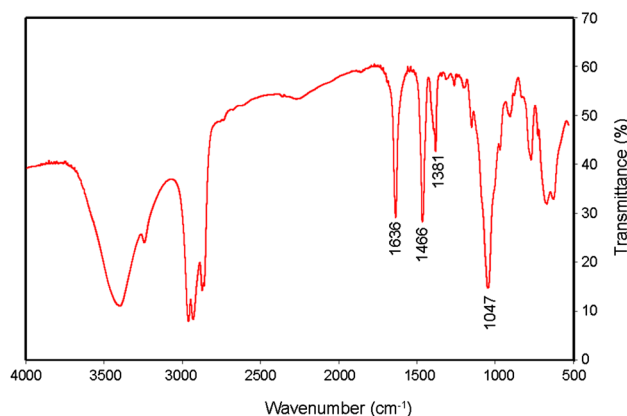**Fig. 4** IR spectrum of Mg(OR)$_2$ after exposure to air. Absorption between 3200 and 3500 cm^{-1} and a new peak at 1636 cm^{-1} are clear signs of the presence of moisture

exhibited regular hydrocarbon absorption between 2800 and 3000 cm^{-1} and two individual peaks at 1378 and 1462 cm^{-1} and the absorbed carbon dioxide showed an absorption peak at 2300 cm^{-1}.

After recording the IR spectrum of the Mg(OR)$_2$ complex, the sample was left in the instrument for a few minutes, and then a second IR spectrum of the complex was recorded, which is shown in Fig. 4.

For a short time the Mg(OR)$_2$ sample was exposed to ambient air and strongly affected its IR absorption spectrum. A broad absorption band of free water or –OH groups between 3200 and 3500 cm^{-1} and a single additional absorption peak at 1636 cm^{-1} can be seen. The hydrocarbon peaks between 2800 and 3000 cm^{-1} and at 1381 and 1466 cm^{-1} were not affected, but the Mg–O–CH$_2$– peak position shifted significantly to the right (lower wavelength) to 1047 cm^{-1}. This indicated that the adsorbed moisture had weakened the Mg–O–CH$_2$– bond and caused the shift
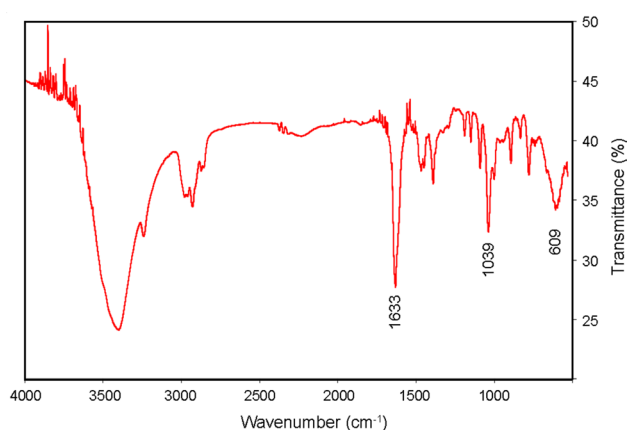

Fig. 5 IR spectrum of pure MgCl$_2$, showing strong absorption at 1633 cm^{-1} and absorption peaks at 1039 and 609 cm^{-1}. The peaks between 3200 and 3500 cm^{-1} indicate moisture adsorption

to a lower energy level. These results show that magnesium compounds easily adsorb moisture from ambient air, which changes the nature of the absorbing Mg compound considerably. The new peak at 1636 cm^{-1} might originate from H$_2$O that is in complexation with magnesium. This absorption peak at 1636 cm^{-1} corresponded to the absorption peak at 1632 cm^{-1} that was reported in the investigations by Thongdonjui et al. and Zohuri et al. [19, 35] describing the IR-absorption of Mg(OEt)$_2$. Our results can indicate that the Mg(OEt)$_2$ investigated by Thongdonjui et al. and Zohuri et al. could have been contaminated by moisture.

IR results for precipitated MgCl$_2$

The KBr tablet containing the MgCl$_2$ precipitate exhibited a strong absorption peak at 1633 cm^{-1} and peaks due to moisture adsorption and of the remaining hydrocarbons. Additional absorption peaks were found at 1039 and 609 cm^{-1} in the spectrum of the neat MgCl$_2$ (Fig. 5). Two publications support the assumption that the Mg–Cl group is the cause of the absorption peak at 1633 cm^{-1}. According to Sinthusai et al. [18] and to Thongdonjui et al. [19], Mg–Cl stretching results in a weak absorption at 2253 and 1852 cm^{-1} and a strong absorption at 1633 cm^{-1} in a ZN catalyst system that very much resembles the system we investigated in this work. According to Zohuri et al. [36], strong absorption of the Mg–Cl group that depends on the nature of the catalyst can be seen in the area between 1590 and 1614 cm^{-1} in a silica-based Ziegler–Natta catalyst, which indicates that the Mg–Cl bond is weakened due to a complex forming between the MgCl$_2$ and the SiO$_2$ carrier. They suggested that the absorption peak at 1633 cm^{-1} was caused by the Mg–Cl group, but—as can be seen from the experimental results described above—this peak can also be caused by adsorbed moisture.

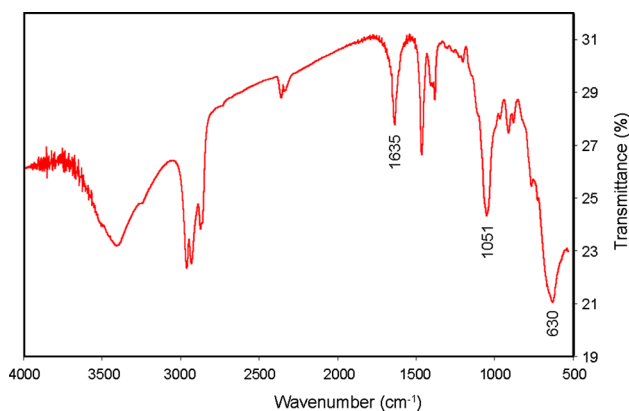**Fig. 6** IR spectrum of MgCl$_2$-EtAl(OR)$_2$, showing Mg–Cl/moisture absorption at 1635 cm^{-1}, the Al–O–CH$_2$– group at 630 cm^{-1}, and a peak at 1051 cm^{-1}. In addition, the normal hydrocarbon and –OH/H$_2$O absorption peaks can be seen in the spectrum

Fig. 7 Schematic drawing showing the possible locations of the bonds responsible for the absorption peaks at 630–635, 1045–1051 and 1633–1635 cm^{-1}

IR results of the MgCl$_2$-EtAl(OR)$_2$ and the MgCl$_2$-TiCl$_3$(OR) model compounds

MgCl$_2$-EtAl(OR)$_2$ also showed a strong absorption peak at 1635 cm^{-1}, which indicated the presence of a Mg–Cl/moisture bond. Two additional absorption peaks appeared at 1051 and at 630 cm^{-1} (Fig. 6). The absorption at 630 cm^{-1} can be related to the free Al–O–CH$_2$– groups, as they exhibited absorption at 635 cm^{-1} in all model compounds. The absorption at 1051 cm^{-1} may have originated from the same group in a strong complex with magnesium forming a Mg–O(Al)–CH$_2$ complex and may even include a shift of a chlorine group from Mg to Al. Figure 7 shows the assumed locations of the absorption peaks. The MgCl$_2$-TiCl$_3$(OR) complex also shows a strong Mg–Cl/moisture absorption at 1635 cm^{-1}, and additional peaks at 1073 and 603 cm^{-1}. Logically, the 603 cm^{-1} absorption must originate from Mg–O–CH$_2$– group, since for the model compound, the Mg–O–CH$_2$– group showed an absorption at 595 cm^{-1}. If this is the case, then a part of the –OR groups from the titanium compound must have shifted to magnesium according to:

$$MgCl_2 + TiCl_3(OR) \rightarrow ClMgOR + TiCl_4 \qquad (7)$$

However, since the absorption peak for the Mg–Cl group remained strong, only few of the –OR groups must have shifted toward magnesium. The third absorption peak at 1073 cm^{-1} resulted most likely from the Ti–OR group coordinated to MgCl$_2$.

IR Results for the MgCl$_2$ support material

IR Spectra of several MgCl$_2$ support materials were taken. In the measurements, we used KBr tablets. All support materials exhibited strong absorption at 1635 cm^{-1}, which
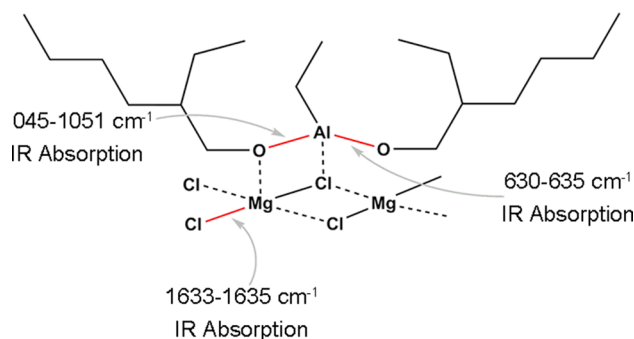
originated from the Mg–Cl bond. This is in good agreement with what we observed for the MgCl$_2$ and MgCl$_2$-EtAl(OR)$_2$ model compounds which also accords with reports in the literature [18, 19]. Another distinct absorption peak was detected at 1045 cm^{-1}. This may correspond to the absorption of the Mg–O–Al–CH$_2$– group seen in the MgCl$_2$-EtAl(OR)$_2$ model compound. In addition, there was a clear but somewhat broader peak between 630 and 670 cm^{-1}, which fitted with the strong absorption at 635 cm^{-1} of the free Al–O–CH$_2$– group seen in the MgCl$_2$–EtAl(OR)$_2$ model compound and in the EtAl(OR)$_2$ and Al(OR)$_3$ model compounds. Hence, it can be concluded that the support material produced closely resembles the MgCl$_2$–EtAl(OR)$_2$ model compound in Fig. 6.

The n-heptane solution remaining in the catalyst showed absorption between 2900 and 2967 cm^{-1} and two separate peaks at 1465 and 1380 cm^{-1}, which is in agreement with reports by Blitz et al., Deslauriers et al. and Thushara et al. [34, 37, 38].

The spectrum of the support material featured a large absorption band between 3200 and 3500 cm^{-1} with a maximum at 3446 cm^{-1}. This absorption was in accordance with the results of Chien et al. [39], who reported for moisture-contaminated Ziegler–Natta catalysts a broad absorption band between 3350 and 3320 cm^{-1} originating from –OH groups and an absorption peak at 3570 cm^{-1} resulting from free water. In our case, the absorption originated from moisture, adsorbed by the support material, when the IR tablet was moved from the press to the IR instrument. Additional water may have originated from an internal equilibrium reaction as it is illustrated in Fig. 8.

IR Results for the catalyst

In order to prepare KBr tablets for the IR measurements, we ground 2 mg of the catalyst together with 200 mg of KBr in a glove box and placed the powder between the
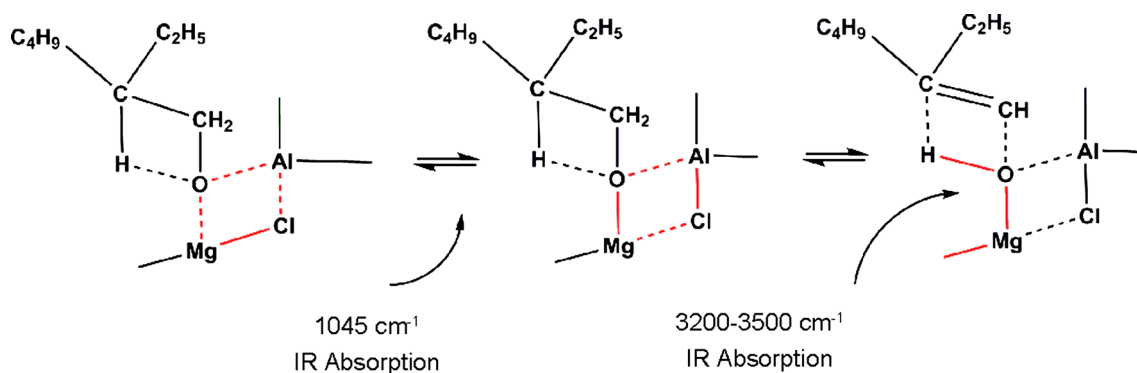
Fig. 8 Possible equilibrium reaction at the position of the –OR group on an Mg–Al adduct

clams of a tablet press. The clams were quickly taken to the laboratory, where force was applied to the press to obtain the KBr tablet, which was immediately transferred to the measuring instrument to minimize adsorption of moisture from ambient air. Nonetheless, the spectra (Fig. 9) show a clear absorption band between 3200 and 3500 cm^{-1}, which indicates the presence of moisture. It is possible to increase the height of the Mg–Cl absorption peak at 1633–1635 cm^{-1} due to moisture adsorption. A separate peak to the right of the main moisture peak is detected at 3241 cm^{-1} which may originate from the moisture and form a complex with MgCl$_2$, because, according to Rönkkö et al. the peaks of free –OH groups and moisture peaks tend to shift to the right when a complex is formed with MgCl$_2$ [40]. As the catalyst had been a slurry in *n*-heptane, the spectra also showed absorption due to remaining *n*-heptane between 2873 and 2961 cm^{-1}, and two separate peaks at 1381 and 1464 cm^{-1}. However, the *n*-heptane absorption did not dominate the spectra. The catalysts showed strong absorption at 1634–1635 cm^{-1} corresponding to the Mg–Cl bond. These bands were in accordance with the findings by Sinthusai et al. and by Thongdonjui et al. [18, 19]. One of the Ti–Cl absorption peaks may have appeared in some of the catalyst IR spectra that showed absorption between 603 and 617 cm^{-1}. This would correspond to the Ti–Cl absorption at 618 cm^{-1} reported by Thongdonjui et al., though these results should not be regarded as conclusive. The main absorption peak of Ti–Cl at 466 cm^{-1} was too close to the measurement limit of the instrument, so it could not be identified. Additionally, there was a strong absorption peak at 1045 cm^{-1} [19] which corresponded to that seen in the support material and was assumed to originate from the complex between the EtAl(OR)$_2$ and the MgCl$_2$ carrier material. The only indication of the presence of titanium in the catalyst was the absorption peak at 617 cm^{-1}.

On the basis of these results, it can be concluded that there is a strong resemblance between the IR spectra of the support material and that of catalyst. Both showing the
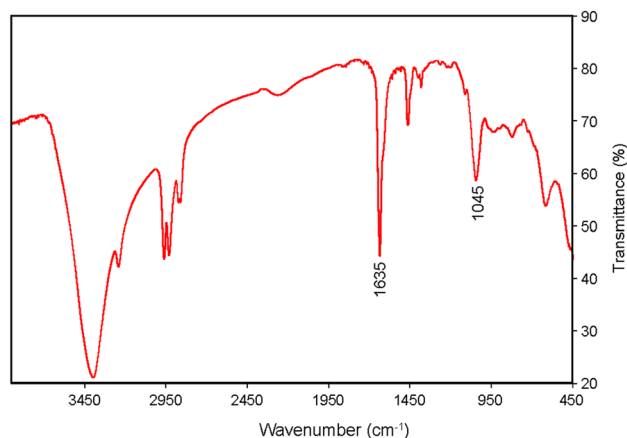

Fig. 9 Example IR spectrum of catalyst 0105-1, showing the distinct absorption peak of Mg–Cl at 1635 cm^{-1} and the absorption peak at 1045 cm^{-1} originating from the complex between EtAl(OR)$_2$ and MgCl$_2$

same structure which suggests that the base material in the catalyst consists of MgCl$_2$ to which EtAl(OR)$_2$ is coordinated. There is no clear sign of the presence of titanium compounds, as the main absorption peaks of Ti–Cl are outside the measuring limits of the IR instrument used. Nor is there any sign of a Cl$_3$Ti–OR compound, which should, according to the model compound 1206-2, exhibit a strong absorption peak at 1073 cm^{-1}. This suggests that there is no significant shift of –OR groups from the EtAl(OR)$_2$ compound to TiCl$_4$. The fact that most or all of the titanium was in the form of TiCl$_4$ in this catalyst, and thereby outside the range of the measuring instrument, can explain why no titanium could be detected in the IR-spectra of the catalysts even if the catalyst contained 4 w% of titanium. It also indicates that there was no reaction between adsorbed H$_2$O and TiCl$_4$ in these catalysts as this would have created Ti–OH groups or even Ti–O–Ti groups that should have shown up in the IR-spectra. This has a practical consequence, since, according to Salajka et al. RO-groups on titanium cause

Table 4 Reproducibility of crystal thickness in a standard synthesis where Mg(OR)$_2$ was added over a period of 20 min at 60 °C and the EtAlCl$_2$/Mg(OR)$_2$ molar ratio was 1:1

Catalyst code	Synthesis conditions	FWHM (°)	2θ (°)	FWHM (rad)	Crystallite size (Å)
2105-1	Standard	1.3271	50.6903	0.023165268	71
0206-2	Standard	1.3813	50.6431	0.024111359	68

The titanation temperature was 60 °C, and there was no second titanation step

often the catalyst to yield a polymer with lower molecular weight and a somewhat broader molecular weight distribution (MWD) than TiCl$_4$ [41–43]. According to Wolf et al., –OR groups on titanium can also result in R-Cl splitting off and formation of either Ti–O–Ti or Ti=O groups in the catalyst [29, 44]. The large absorption band around 3500 cm^{-1} that is seen in all catalyst IR-spectra is typical for MgCl$_2$ based Ziegler–Natta catalysts. This absorption band originates from adsorbed H$_2$O on the active MgCl$_2$ carrier. The reason why this adsorbed moisture is not reacting with the TiCl$_4$ in the catalyst creating Ti–OH groups or Ti–O–Ti bonds that could immediately appear in a reaction between free TiCl$_4$ and H$_2$O is not known.

X-ray results

In our study, XRD of the prepared catalysts generally showed a small reflection peak at 2θ = 15°, further—partly merged—reflection peaks at 2θ = 30° and 2θ = 35°, and a peak at 2θ = 50°. This is in agreement with results described in the literature about the small reflection peak at 2θ = 15° [1, 15] and the partly merged—reflection peaks at 2θ = 30° and 2θ = 35° [45–47].

Some publications have described MgCl$_2$ crystal thickness: Nakayama et al. [21]. prepared support material with a thickness of 28 Å, Chien et al. [48] produced a ball-milled catalyst with a crystal thickness of 36 Å, Busico et al. [28] prepared a PP catalyst with a crystal thickness of 130 Å, Singh et al. [49] synthesized a similar kind of catalyst with a crystal thickness of 31 Å, and Kojoh et al. [50] described their use of TiCl$_4$ to hinder MgCl$_2$ from forming larger crystals in precipitation reactions.

Reproducibility of the synthesis in terms of crystal thickness

A so-called standard synthesis was repeated in order to determine to what degree the thickness of the catalyst crystals was reproducible in parallel catalyst syntheses. In the standard synthesis, the Mg(OR)$_2$ was added within 20 min at 60 °C, and the EtAlCl$_2$/Mg(OR)$_2$ molar ratio was 1:1. The titanation temperature was 60 °C, and there was no second titanation. The results from these two standard syntheses are listed in Table 4. The thickness of the MgCl$_2$ crystal was calculated from the reflection peak at 2θ = 50°, on which our study concentrated. Given the peak
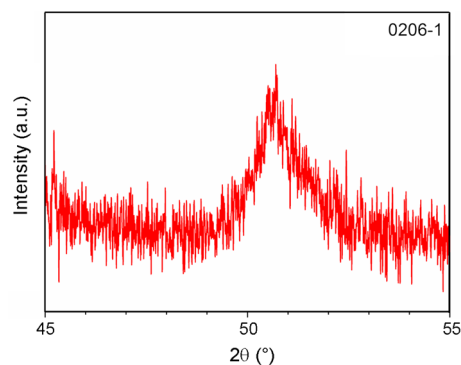

Fig. 10 XRD measurement between 45° 2θ and 55° 2θ of standard catalyst 0206-1 from a synthesis in which Mg(OR)$_2$ was added over 20 min at 60 °C and the EtAlCl$_2$/Mg(OR)$_2$ molar ratio was 1:1. The titanation temperature was 60 °C, and there was no second titanation

position, the most probable crystalline phase is rhombohedral MgCl$_2$. However, due to the relatively small difference (approximately 0.3°) in the 2θ positions between the rhombohedral and hexagonal phases and the significant peak broadening caused by the small crystallite size, the presence of a hexagonal phase cannot be completely excluded. Thus, most diffractograms were measured only between 2θ ranging from 45° to 55° (Fig. 10). The results show that both measurements yielded a crystal thickness close to 70 Å, which corresponds to an acceptable maximum error of 5 %.

Change in MgCl$_2$ crystal thickness due to titanation

To determine to what extent the TiCl$_4$ treatment of the support material influenced MgCl$_2$ crystal thickness, XRD measurements of the support material (0206-1s) and of the final catalyst (0206-2) after TiCl$_4$ treatment were taken. The results listed in Table 5 show that the TiCl$_4$ treatment of the support material caused an increase in MgCl$_2$ crystal thickness from 60 Å to almost 68 Å.

Influence of the temperature during synthesis on crystal thickness

In order to observe the effect of the temperature during synthesis on the crystal size of the MgCl$_2$ carrier material, we prepared a series of catalysts at different temperatures within the range from 40 to 120 °C. At 120 °C,

Table 5 Crystal thickness of the support material and of the corresponding catalysts measured by X-ray diffraction at 50° 2θ. The support material and the catalyst were prepared at 60 °C

Code	Target	Crystallite size (Å)
0206-1s	Support	60
0206-2	Catalyst	68

Table 6 Thickness of catalyst crystals prepared at different temperatures and measured by X-ray diffraction at 2θ = 50°

Catalyst code	Catalyst synthesis temperature (°C)	Crystallite size (Å)
1006-2	40	44
0206-2	60	68
0606-1	70	64
1006-1	90	59

Fig. 11 The MgCl$_2$ crystal thickness measured at 2θ = 50° is correlated to the synthesis temperature during preparation of the MgCl$_2$ support material

Fig. 12 X-ray diffraction of the 0406-1 catalyst prepared at 120 °C, showing changes in the crystalline phase and/or orientation indicated by the presence of another reflection at approximately 2θ = 52.3°

Table 7 Thickness of catalyst crystals for different Mg(OR)$_2$ addition times (for 60 °C synthesis temperature and an EtAlCl$_2$/Mg(OR)$_2$ molar ratio of 1:1)

Catalyst code	Mg(OR)$_2$ addition time (min)	Crystallite size (Å)
1405-1	1	49
2105-1	20	71
0206-2	20	68
1205-1	120	74
1905-1	300	64

the synthesis had to be carried out in a nonane solution to prevent the reaction solution from boiling. After preparation, the thickness of the catalyst crystals was measured by XRD. The results listed in Table 6 show that the largest crystals (around 68 Å) were formed at 60 °C. At lower temperatures, crystal size decreased dramatically, dropping to 44 Å at 40 °C. The decrease in crystal size when using higher synthesis temperatures can be explained by the normal tendency of creating smaller crystal size when the precipitation reaction is increased due to higher and faster reaction rate leading to a faster over saturation of the precipitating product giving smaller crystal size. The decrease in crystal size when using lower synthesis temperature can only be explained by a slower chlorination reaction of Mg(OR)$_2$ by EADC leading to an insufficient crystal growth.

A gradual decrease in crystal size was also observed at higher temperatures: at about 90 °C, the crystals had a thickness of about 59 Å (Fig. 11; Table 6). At even higher temperatures, a partial change in the crystal structure occurred, as indicated by the development of another reflection peak in the XRD pattern (Fig. 12). The second peak found at approximately 2θ = 52.3° might be related either to the development of hexagonal MgCl$_2$ in addition to the rhombohedral one or to an increase in crystals with different orientations compared to the rhombohedral phase.

Influence of the addition time of Mg(OR)$_2$ on crystal thickness

In order to investigate to what extent it is possible to influence MgCl$_2$ crystal thickness by changing the Mg(OR)$_2$ addition time, we carried out a series of syntheses where

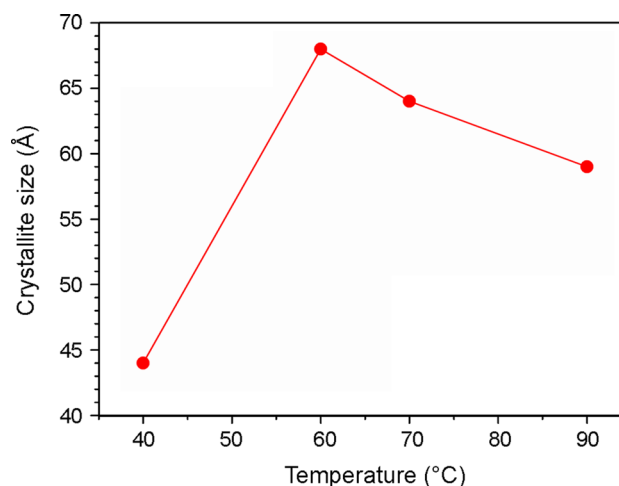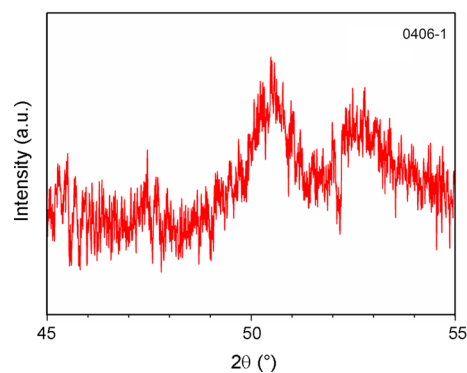the Mg(OR)$_2$ addition time was changed from 1 to 300 min. Otherwise, standard conditions were used (synthesis at 60 °C with an EtAlCl$_2$/Mg(OR)$_2$ molar ratio of 1:1 and no second titanation). The results (Table 7) show that the crystal size of the MgCl$_2$ support increases minimally with

Table 8 Effect of (1) increased amount of EtAlCl$_2$ in the catalyst synthesis and (2) a second TiCl$_4$ treatment on the thickness of MgCl$_2$ crystal plates

Catalyst code	Synthesis modification	Crystallite size (Å)
1106-1	Double EtAlCl$_2$	69
1706-1	Second TiCl$_4$ step	63

increasing Mg(OR)$_2$ addition time. Extending the addition time from 20 min to 2 h resulted in a crystal thickness that increased from approximately 71–74 Å. For even longer addition times the crystals became narrower. The same was the case when the addition times were shorter than 20 min.

*Influence of EtAlCl$_2$/Mg(OR)$_2$ molar ratio or a second titanation on crystal thickness*

Next we sought to assess whether it is possible to modify the thickness of the MgCl$_2$ crystals through stronger chlorination. We carried out two syntheses at 60 °C with a Mg(OR)$_2$ addition time of 20 min: In the first, the EtAlCl$_2$/Mg(OR)$_2$ molar ratio was increased from 1:1 to 2:1, and in the second a second titanation with a TiCl$_4$/MgCl$_2$ molar ratio of 12:1 was introduced. Neither resulted in a significant increase in crystal thickness (Table 8). In the case in which the EtAlCl$_2$/Mg(OR)$_2$ molar ratio was doubled, the carrier had nearly the same crystal thickness (69 Å) as observed in the standard synthesis of 0206-2 catalyst (68 Å). In the case of a second TiCl$_4$ treatment of the catalyst, a slightly smaller crystal size of 63 Å was achieved.

SEM results

In a typical Ziegler–Natta catalyst, the particles usually have a size of 20–30 µm. The particles are formed by clusters of nanoparticles of about 100 nm. The SEM images in our study were used to describe the physical appearance of the catalyst and to investigate whether the changes in the catalysts synthesis conditions caused any clear changes in the inner structure of the catalyst.

First, we compared the SEM pictures of the catalysts synthesized with different addition times of magnesium alcoholate to the solution of EADC. We found that increasing the addition time resulted in larger catalyst nanoparticles of up to 200 nm. This trend was observed for 1, 20 min and 2 h addition time. For even longer addition times, no further increase in nanoparticle size could be identified.

Our comparison of the SEM pictures of the catalysts prepared at different temperatures showed that the largest nanoparticles, in the range of 200–300 nm (Fig. 13), were obtained at 60 °C. For higher or lower temperatures, nanoparticle size decreased to approximately 100 nm (Fig. 14).
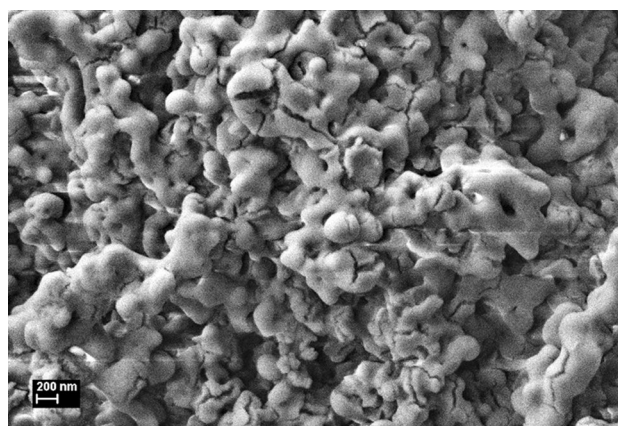
Fig. 13 SEM picture of the catalyst produced at 60 °C with a Mg(OR)$_2$ addition time of 20 min showing a nanoparticle size of around 200 nm
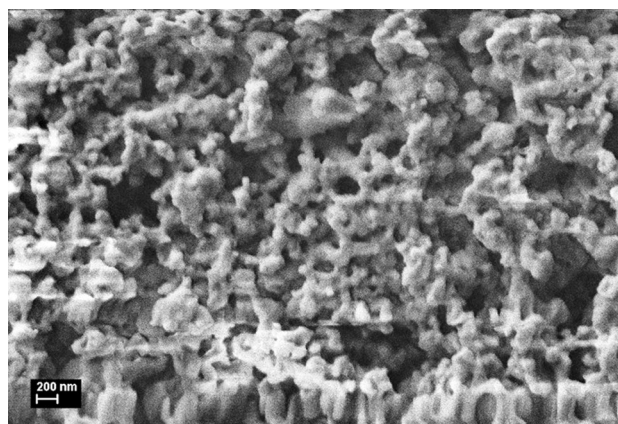
Fig. 14 SEM picture of the catalyst produced at 120 °C with an addition time of 20 min showing a nanoparticle size of around 100 nm

Table 9 Nanoparticle size determined based on SEM pictures of catalysts prepared at different temperatures

Synthesis temperature (°C)	Nanoparticle size (nm)
60	200–300
80	150–200
100	100–150
120	80–100

Nanoparticle size of catalysts prepared at a temperature of 40 °C seemed larger than that of particles prepared at 120 °C (Table 9.).

Further, the SEM pictures showed that the EtAlCl$_2$/Mg(OR)$_2$ molar ratio had no impact on nanoparticle size.

The relationships between nanoparticle size, addition time and synthesis temperature as identified from SEM pictures correlate with those determined by XRD.
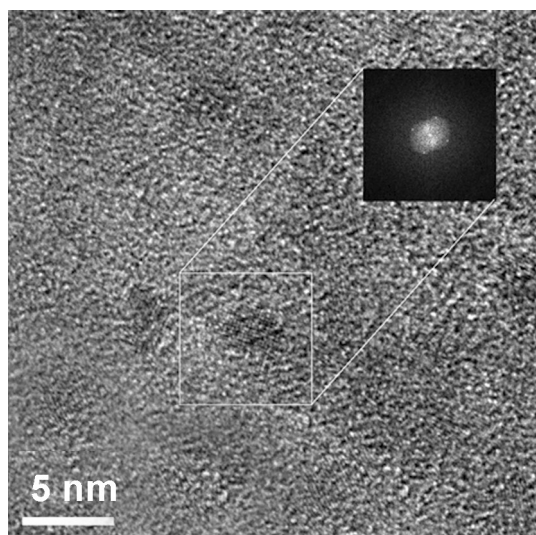
Fig. 15 TEM picture showing the size of the individual $MgCl_2$ crystals in a Ziegler-Natta catalyst

TEM results

We recorded TEM images for selected catalyst samples. Figure 15 shows a typical example image from our study, where the crystalline $MgCl_2$ discs forming the base units of the crystalline material can be seen. The size of these base units varied between 4 and 7 nm. The TEM image of the 0206-2 catalysts (Fig. 15) showed crystallite sizes in the range of 5–6 nm. These results are therefore in good agreement with those calculated from the XRD patterns.

Estimating the physical composition of the catalyst

XRD measurements showed that the thickness of the $MgCl_2$ crystals was around 7 nm, which gave a plate radius of 3.5 nm. Should five crystal plates stacked on top of each other form a base unit, it has a volume that roughly corresponds to that of a sphere with a radius of 3.5 nm. The volume therefore amounts to $3\pi/4 \times (3.5 \text{ nm})^3$. Our SEM pictures showed that the nanoparticles had a diameter of 200 nm, which corresponded to a volume of $3\pi/4 \times (100 \text{ nm})^3$. Dividing this volume by the volume of the base unit, we find that around 25 000 base units can be fitted into one nanoparticle, leading to about 125 000 $MgCl_2$ crystal plates per nanoparticle. As the yield of the catalyst synthesis was about constant it could be assumed that the smaller the crystal size was, the greater number of crystals was needed to make up the same yield.

Catalyst particles commonly have a size of 20 μm, which corresponds to a volume of $3\pi/4 \times (10\ 000 \text{ nm})^3$. Dividing this volume by the volume of the nanoparticle yields one million. The calculation thus shows that a 20 μm Ziegler–Natta catalyst particle contains about one million nanoparticles, each of which consists of about 105 of $MgCl_2$ crystal plates (Fig. 16). The absolute particle size of the catalyst could only visually be estimated in our investigation. This was done from the microscope pictures. The catalyst particles did not have a regular shape

and many times it was difficult to judge if a particle was consisting of a cluster or of a single particle. This is a common feature for the precipitated Ziegler–Natta catalysts where there has been no directing force in connection to the preparation of the $MgCl_2$ support material. Therefore, only an indicative estimation of the relation between the $MgCl_2$ crystal size and the catalyst particle size can be made. This estimation indicated that if higher temperatures had been used in the synthesis, the catalysts tended to be somewhat bigger. The catalyst showed then also a more regular morphology having a higher bulk density. The catalyst prepared at 40 °C showed clearly a smaller particle size and also a smaller $MgCl_2$ crystal broadness.

In general it can be said that the better morphology a catalyst possesses, the better is the physical strength of the catalyst particle which in turn gives a better morphology to the produced polymer. A correlation between the crystal size and strength of the catalyst particles could be seen only when using lower synthesis temperatures. Then a smaller crystal size was created and at the same time a worse morphology of the catalyst which in turn led to a weaker catalyst particle that in turn created a worse morphology to the produced polymer. No physical tests were however done to measure the catalyst particle strength in connection to this investigation.

Polymerization quick test

Figure 17 illustrates an example of this polymerization quick test where catalyst 1205-1 was polymerized. The test clearly shows that the size of the studied particle increases from the initial size of 53–284 μm after 30 min of polymerization and thus that the catalyst contains active titanium. All catalysts produced were tested with this procedure and showed reasonable growth, which indicated that they all contained active titanium. In our polymerization quick tests we could not see any difference in catalyst activity that would correspond to the $MgCl_2$ crystal thickness of the catalyst. In literature no systematic study focusing on the correlation between the catalyst $MgCl_2$ crystal thickness and the activity of the catalyst could be found.

Conclusion

This study investigated how changes in the synthesis conditions alter the crystal thickness of a typical $MgCl_2$-based PE Ziegler–Natta catalyst. The $MgCl_2$ support material was

$$V = \frac{3}{4} \cdot r^3 \cdot \pi$$

$$V = \frac{3}{4} \cdot \left(100 \cdot 10^{-9}\right)^3 \cdot \pi$$

$$V = 10^6 \cdot 10^{-27} \cdot \frac{3}{4}\pi$$

Nanoparticle contains 25 000 crystals

Particle contains 1 000 000 nanoparticles

← 200 nm →

Nanoparticle
SEM

7 nm

$$V = \frac{3}{4} \cdot r^3 \cdot \pi$$

$$V = \frac{3}{4} \cdot \left(3,5 \cdot 10^{-9}\right)^3 \cdot \pi$$

$$V = 42,875 \cdot 10^{-27} \cdot \frac{3}{4}\pi$$

MgCl₂ crystal
XRD

20 µm

$$V = \frac{3}{4} \cdot r^3 \cdot \pi$$

$$V = \frac{3}{4} \cdot \left(10000 \cdot 10^{-9}\right)^3 \cdot \pi$$

$$V = 10^{12} \cdot 10^{-27} \cdot \frac{3}{4}\pi$$
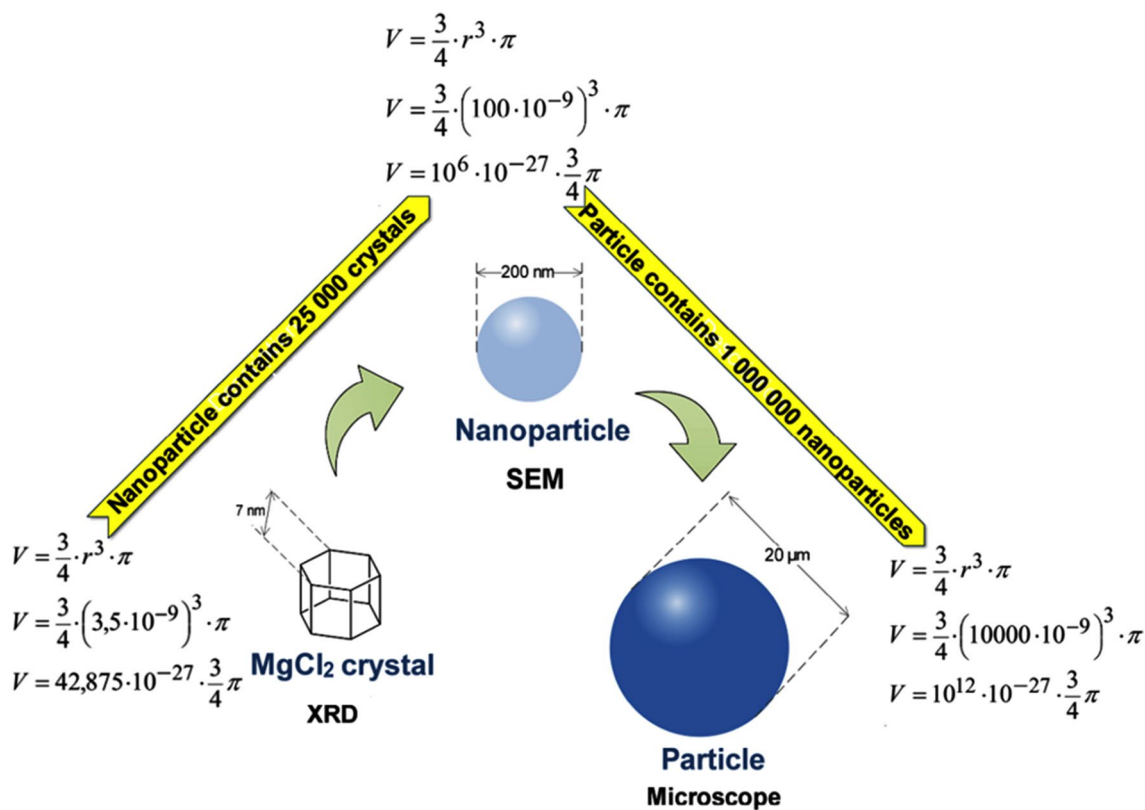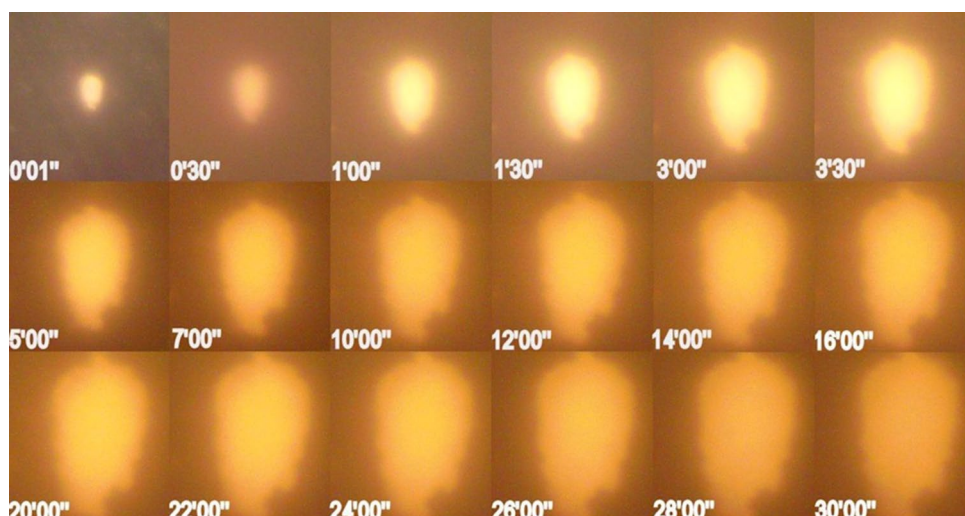
Particle
Microscope

Fig. 16 The physical composition of a 20 µm Ziegler-Natta catalyst particle. The catalyst particle contains about one million nanoparticles, each of which consists of about 25 000 of $MgCl_2$ crystal units that contain five $MgCl_2$ crystal plates

Fig. 17 Example of polyethylene formation in the polymerization quick test. The tested catalyst 1205-1 was prepared at 60 °C with a Mg(OR)₂ addition time of 120 min

0'01"   0'30"   1'00"   1'30"   3'00"   3'30"
5'00"   7'00"   10'00"   12'00"   14'00"   16'00"
20'00"   22'00"   24'00"   26'00"   28'00"   30'00"

created by adding $Mg(OR)_2$ to $EtAlCl_2$. $TiCl_4$ was added after the support material had been washed. The thickness of the catalysts was measured by X-ray diffraction using the reflection at $2\theta = 50°$. The results were confirmed by means of TEM pictures. To determine whether a correlation exists between $MgCl_2$ crystal thickness and nanoparticle size, we took SEM pictures of the catalysts, based on which the

nanoparticle size could be estimated. IR spectroscopy was employed to determine the chemical composition of the catalysts. In summary, the results of these investigations were:

- Overcoming the settling problems in the synthesis process by using a catalyst synthesis reactor that could be transferred to a centrifuge both accelerated production

significantly and introduced a high degree of precision to the process.

- The IR results for the MgCl$_2$-EtAl(OR)$_2$ model compound indicated that an exchange of Cl and –OR groups between Mg and Al may occur.

- The IR results for the MgCl$_2$–Cl$_3$Ti–OR model compound indicated that an exchange of Cl and –OR groups between Mg and Ti was possible.

- The IR spectra also revealed that there is a strong resemblance between the chemical composition of the support material and that of the catalyst, which suggests that the base material in the catalyst consists of MgCl$_2$ in coordination equilibrium with Mg(OR)$_2$ and EtAl(OR)$_2$. The IR results gave no clear indication of the presence of titanium compounds in the catalyst.

- According to the XRD results, there was an increase from 60 Å to almost 68 Å in MgCl$_2$ crystal thickness due to the TiCl$_4$ treatment of the support material.

- The XRD results showed that the largest crystals (70 Å) were created at a synthesis temperature of 60 °C. For lower temperatures, the crystal size decreased dramatically to only about 44 Å at 40 °C. A gradual decrease in crystal size was also observed for higher temperatures: at 90 °C a crystal thickness of about 59 Å was obtained. For even higher temperatures, an additional peak appeared in the diffraction pattern.

- The XRD results showed that increasing the addition time of Mg(OR)$_2$ results in only a minor increase in crystal size of the MgCl$_2$ support material.

- The XRD results further revealed that increased chlorination by higher amounts of EtAlCl$_2$ or TiCl$_4$ did not cause a significant change in the thickness of MgCl$_2$ crystals.

- The TEM pictures confirmed that the size of the MgCl$_2$ crystals was between 40 and 70 Å.

- Our SEM pictures showed that there was a slight correlation between MgCl$_2$ crystal thickness and nanoparticle size. Nanoparticles of 200 nm and about 100 nm were obtained at synthesis temperatures of 60 and 100 °C, respectively.

- Our calculation showed that a 20 µm Ziegler–Natta catalyst particle contained about one million nanoparticles, each of which consisted of about 105 MgCl$_2$ crystal plates.

- All catalysts showed chemical activity in a polymerization quick test.

This investigation was planned as the first of a series of studies in which we have sought to reveal correlations between the thickness of the MgCl$_2$ support material in a typical polyethylene Ziegler–Natta catalyst and its co-polymerization performance. As part of future work, we will evaluate the effect of MgCl$_2$ crystal thickness on polymerization activity, molecular weight capability, width

of molecular weight distribution, and amount of soluble polymer material in co-polymers, especially when higher amounts of co-monomer are incorporated.

References

1. Kashiwa N (2004) The discovery and progress of MgCl$_2$-supported TiCl$_4$ catalysts. J Polym Sci Part A Polym Chem 42:1–8

2. Galli P, Vecellio G (2001) Technology: driving force behind innovation and growth of polyolefins. Prog Polym Sci 26:1287–1336

3. Vaughan A, Davis DS, Hagadorn JR (2012) Industrial catalysts for alkene polymerization. Polym Sci A Compr Ref 3:657–672

4. Kissin YV (2012) Active centers in Ziegler-Natta catalysis: formation kinetics and structure. J Catal 292:180–200

5. Kebritchi A, Nekoomanesh M, Mohammadi F (2015) The interrelationship between microstructure and melting, crystallization and thermal degradation behaviours of fractionated ethylene/1-butene copolymer. Iran Polym J 24:267–277

6. Nouri M, Parvazinia M, Arabi H (2015) Effect of fragment size distribution on reaction rate and molecular weight distribution in heterogeneous olefin polymerization. Iran Polym J 24:437–448

7. Bahri-Laleh N, Correa A, Mehdipour-Ataei S, Arabi H, Haghighi MN, Zohuri G, Cavallo L (2011) Moving up and down the titanium oxidation state in Ziegler-Natta Catalysts. Macromolecules 44:778–783

8. Stukalov DV, Zakharov VA (2009) Active site formation in MgCl$_2$-supported Ziegler-Natta catalyst. A density functional theory study. J Phys Chem C 113:21376–21382

9. Mikenas TB, Koshevoy EI, Zakharov VA, Nikolaeva MI (2014) Formation of isolated titanium(III) ions as active sites of supported titanium-magnesium catalysts for polymerization of olefins. Macromol Chem Phys 215:1707–1720

10. Soares JBP, McKenna TFL (2012) Polyolefin Reaction Engineering. Wiley-VCH, Weinheim

11. Kissin YV, Mink RI, Brandolini AJ, Nowlin TE (2009) AlR$_2$Cl/MgR$_2$ combinations as universal co-catalysts for Ziegler-Natta, metallocene, and post-metallocene catalysts. J Polym Sci A Polym Chem 47:3271–3285

12. Boero M, Parrinello M, Hüffer S, Weiss H (2000) First principles study of propene polymerization in Ziegler-Natta heterogeneous catalysis. J Am Chem Soc 122:501–509

13. Cipullo R, Mellino S, Busico V (2014) Identification and count of the active sites in olefin polymerization catalysis by oxygen quench. Macromol Chem Phys 215:1728–1734

14. Liu Z, Zhang X, Huang H, Yi J, Liu W, Liu W, Zhen H, Huang O, Gao K, Zhang M, Yang W (2012) Synthesis of (co-)polyethylene with broad molecular weight distribution by the heterogeneous Ziegler-Natta catalysts via one-pot strategy. J Ind and Eng Chem 18:2217–2224

15. Di Noto V, Zanetti R, Viviani M, Marega C, Marigo A, Bresadola S (1992) MgCl$_2$-supported Ziegler-Natta catalysts: a structural

investigation by X-ray diffraction and Fourier-transform IR spectroscopy on the chemical activation process through $MgCl_2$-ethanol adducts. Makromol Chem 193:1653–1663

16. Dwivedi S, Taniike T, Terano M (2014) Understanding the chemical and physical transformations of a Ziegler-Natta catalyst at the initial stage of polymerization kinetics: the key role of alkylaluminum in the catalyst activation process. Macromol Chem Phys 215:1698–1706

17. Garoff T, Waldvogel P, Pesonen K (2004) Method for the preparation of olefin polymerization catalyst support and an olefin polymerization catalyst. U.S. Patent 7,432,220

18. Sinthusai L, Trakarnpruk W, Strauss R (2009) Ziegler-Natta catalyst with high activity and good hydrogen response. J Met Mater Miner 19:27–32

19. Thongdonjui A, Trakarnpruk W, Strauss RH (2009) Effect of electron donor on PE polymerization. J Met Mater Miner 19:17–23

20. Wang J, Cheng R, He X, Liu Z, Tian Z, Liu B (2015) A novel $(SiO_2/MgO/MgCl_2) \cdot TiCl_x$ Ziegler-Natta catalyst for ethylene and ethylene/1-hexene polymerization. Macromol Chem Phys 216:1472–1482

21. Nakayama Y, Bando H, Sonobe Y, Fujita T (2004) Development of single-site new olefin polymerization catalyst system using $MgCl_2$-based activators: MAO-free $MgCl_2$-supported FI catalyst systems. Bull Chem Soc Jpn 77:617–625

22. Severn JR, Chadwick JC (2004) MAO-free activation of metallocenes and other single-site catalysts for ethylene polymerization using spherical supports based on $MgCl_2$. Macromol Rapid Commun 25:1024–1028

23. Chien JCW, Wu JC, Kuo CI (1982) Magnesium chloride supported high-mileage catalysts for olefin polymerization. I. Chemical composition and oxidation states of titanium. J Polym Sci Polym Chem Ed 20:2019–2032

24. McKenna TFL, Tioni E, Ranieri MM, Alizadeh A, Boisson C, Monteil V (2013) Catalytic olefin polymerization at short times: studies using specially adapted reactors. Can J Chem Eng 91:669–686

25. Gusev AI, Rempel AA (2004) Nanocrystalline materials. Cambridge International Science Publishing, Cambridge

26. Nejad MH, Ferrari P, Pennini G, Cecchin G (2008) Ethylene homo and copolymerization over $MgCl_2$-$TiCl_4$ catalysts: polymerization kinetics and polymer particle morphology. J Appl Polym Sci 108:3388–3402

27. Pirinen S, Jayaratne K, Denifl P, Pakkanen TT (2014) Ziegler-Natta catalysts supported on crystalline and amorphous $MgCl_2$/THF complexes. J Mol Catal A Chem 395:434–439

28. Busico V, Causà M, Cipullo R, Credendino R, Cutillo F, Friederichs N, Lamanna R, Segre A, Castelli VVA (2008) Periodic DFT and high-resolution magic-angle-spinning (HR-MAS) 1H NMR investigation of the active surfaces of $MgCl_2$-supported Ziegler-Natta catalysts. The $MgCl_2$ matrix. J Phys Chem C 112:1081–1089

29. Zijlstra HS, Stuart MCA, Harder S (2015) Structural investigation of methylalumoxane using transmission electron microscopy. Macromolecules 48:5116–5119

30. Abboud M, Kallio K, Reichert KH (2004) Video microscopy for fast screening of polymerization catalysts. Chem Eng Technol 27:694–698

31. Natter H, Schmelzer M, Löffler MS, Krill CE, Fitch A, Hempelmann R (2000) Grain-growth kinetics of nanocrystalline iron studied in situ by synchrotron real-time X-ray diffraction. J Phys Chem B 104:2467–2476

32. Andoni A (2009) A flat model approach to Ziegler-Natta olefin polymerization catalysts. Doctor Thesis, Technische Universiteit Eindhoven

33. Gupta VK, Satish S, Bhardwaj IS (1993) $MgCl2 \cdot 6H_2O$-based titanium catalysts for propene polymerization. Die Angew Makrom Chem 213:113–125

34. Ault BS (1980) Infrared matrix isolation study of magnesium metal atom reactions. Spectra of an unsolvated Grignard species. J Am Chem Soc 102:3480–3484

35. Deslauriers PJ, Rohlfing DC, Hsieh ET (2002) Quantifying short chain branching microstructure in ethylene 1-olefin copolymers using size exclusion chromatography and Fourier transform infrared spectroscopy (SEC-FTIR). Polymer 43:159–170

36. Zohuri GH, Ahmadjo S, Jamjah R, Nekoomanesh M (2001) Structural study of mono- and bi- supported Ziegler-Natta catalysts of $MgCl_2/SiO_2/TiCl_4$/donor systems. Iran Polym J 10:149–155

37. Blitz JP, Meverden CC, Diebel RE (1998) Reactions of dibutyl magnesium with modified silica gel surfaces. Langmuir 14:1122–1129

38. Thushara KS, Gnanskumar ES, Mathew R, Jha RK, Ajithkumar TG, Rajamohanan PR, Sarma K, Padmanabhan S, Bhaduri S, Gopinath CS (2011) Toward an understanding of the molecular level properties of Ziegler-Natta catalyst support with and without the internal electron donor. J Phys Chem C 115:1952–1960

39. Chien JCW, Wu JC, Kuo CI (1983) Magnesium chloride supported high-mileage catalysts for olefin polymerization. IV. FTIR and quantitative analysis of modifiers in the catalysts. J Polym Sci Polym Chem Ed 21:725–736

40. Rönkkö HL, Knuuttila H, Linnolahti M, Haukka M, Pakkanen TT, Denifl P, Leinonen T (2011) Complex formation and characterization of $MgCl_2$/2-(2-ethylhexyloxy)ethanol adduct. Inorg Chimica Acta 371:124–129

41. Salajka Z, Kratochvíla J, Hudec P, Věčorek P (1993) One-phase supported titanium-based catalysts for polymerization of ethylene. II. Effect of hydrogen. J Polym Sci A Polym Chem 31:1493–1498

42. Kong Y, Yi J, Dou X, Liu W, Huang O, Gao K, Yang W (2010) With different structure ligands heterogeneous Ziegler-Natta catalysts for the preparation of copolymer of ethylene and 1-octene with high comonomer incorporation. Polymer 51:3859–3866

43. Lemos C, Franceschini F, Radtke C, Santos JHZ, Wolf CR (2012) The effect of partial replacement of $TiCl_4$ by $Ti(OR)_4$ on the performance of $MgCl_2$-supported Ziegler-Natta catalysts. Appl Catal A General 423–424:69–77

44. Wolf CR, de Camargo Forte MM, dos Santos JHZ (2005) Characterization of the nature of chemical species of heterogeneous Ziegler-Natta catalysts for the production of HDPE. Catal Today 107–108:451–457

45. Kashiwa N (1980) Super active catalyst for olefin polymerization. Polym J 12:603–608

46. Di Noto V, Bresadola S (1996) New synthesis of a highly active δ-$MgCl_2$ for $MgCl_2/TiCl_4/AlEt_3$ catalytic systems. Macromol Chem Phys 197:3827–3835

47. Rojanotaikul P, Ayudhya SKN, Charoenchaidet S, Faungnawakij K, Soottitantawat A (2012) Preparation of porous anhydrous $MgCl_2$ particles by spray drying process. Eng J 16:109–114

48. Chien JCW, Wu JC, Kuo CI (1983) Magnesium chloride supported high-mileage catalysts for olefin polymerization. V. BET, porosimetry, and X-ray diffraction studies. J Polym Sci Polym Chem Ed 21:737–750

49. Singh G, Kaur S, Makwana U, Patankar RB, Gupta VK (2009) Influence of internal donors on the performance and structure of $MgCl_2$ supported titanium catalysts for propylene polymerization. Macrom Chem Phys 210:69–76

50. Kojoh SI, Fujita T, Kashiwa N (2001) Recent advances in olefin polymerization catalysts based on group 4 transition metals. Recent Res Develop Polym Sci 5:43–58